Fronts and Convective Cold Pools in the Oklahoma Mesonet. Part I: 15-Year Climatology

ANDREW T. LESAGE * AND STEVEN K. KRUEGER

University of Utah, Salt Lake City, Utah

**Corresponding author address:* Andrew Lesage, Department of Atmospheric Sciences, 135 S 1460 E, Rm 819, Salt Lake City, Utah 84112-0110.

E-mail: andy.lesage@utah.edu

ABSTRACT

For over a dozen years the Oklahoma Mesonet network has provided surface observations at over 100 stations. These observations are used to analyze frontal passages and convective cold pools, active regions where precipitation processes are creating near-surface cold air masses. Case studies are detailed and a 15-year climatology of frontal passages and cold pools was computed in this research.

The climatology of front and cold pool data yielded many similarities. Winter has the largest magnitude changes in ΔT and ΔP while spring had the lowest magnitude change in ΔT and summer had the lowest magnitude change in ΔP. Correlations between ΔT and ΔP are lowest in the more convectively active summer season. Convergence is roughly equal ahead of fronts from spring through fall; however, divergence is present in summer frontal passages earlier and stronger compared to the other seasons. Convergence ahead of fronts was roughly the same on average regardless of whether or not a cold pool formed. Fronts and cold pools are most likely to occur in summer and spring with summer having the highest percentage of fronts which lead to cold pools. Fronts and cold pools are substantially more likely to occur during the late afternoon and early evening in the summer; other seasons had a much weaker diurnal cycle with a slight nocturnal increase in frequency. Western Oklahoma had higher frequencies of frontal passages and cold pools than Eastern Oklahoma with frontal passages having the stronger signal.

These findings help identify seasonal, diurnal, and geographic distributions of fronts and cold pools and can be used in modeling studies to better the understanding of cold pool processes and parameterizations.

1. Introduction

A convective cold pool is a region of cold air at the surface in a convectively initiated system. The cooling is a result of evaporative precipitation in the system and can be influenced by downdrafts; however, downdrafts are not a necessary component. A pressure jump is expected as a result of the hydrostatic adjustment to cooling.

Cold pools are a prominent and common feature of convective systems that have been studied for over half a century. Observations from the Thunderstorm Project detailed regions of descending air behind a squall line as a result of evaporative cooling (Newton 1950). Convergence ahead of the leading edge of the cold pool with divergence behind was also noted as a prominent feature in case studies of these squall lines. The results were similar to those observed near Wilmington, Ohio, where pressure jumps, temperature falls, wind shifts, and precipitation features were observed with squall lines (Tepper 1950). Tepper referred to the squall lines as propagating "pressure jump lines".

In his synoptic analysis of squall lines in the Central United States, Fujita identified three main features of a pressure field: the pressure surge line, the thunderstorm high, and the wake depression (Fujita 1955). The pressure surge line marks the leading edge of the thunderstorm and moves in the storm propagation direction. The thunderstorm high, later more commonly known as a mesohigh, is the high pressure region led by the pressure surge line that contains cool downdrafts that spread out upon reaching the surface. The region of surface cooling from these downdrafts is what would become known as the cold pool of the thunderstorm and is often associated with the mesohigh. The wake depression is a region of low pressure, usually behind the thunderstorm high, which forms a pressure dipole with the thunderstorm high.

A gust front, also known as a density current, has been defined as "the leading edge of a mesoscale pressure dome followed by a surge of gusty winds on or near the ground" (Wakimoto 1982). These gust fronts often tilt forward with height due to surface drag effects (Markowski and Richardson 2012). The speed of a gust front propagation increases with a higher horizontal pressure gradient driving the gust front (Seigel and van den Heever 2012).

Cold pools can have a large range of sizes. Those associated with a single cumulonimbus cell have been modeled on the order of 10 km across (Tompkins 2001) while cold pools associated with an MCS can be on the order of 100-400 km wide (Stensrud et al. 1999). Cold pool depths have a wide range as well, from around 1 km up to 4 km (Roux 1988; Weisman and Rotunno 2005). Estimates of cold pool depth have been made using surface pressure perturbations and virtual temperature deficits of the cold pool (Stensrud and Fritsch 1994). In the Tompkins study the simulated cold pools had a mean lifetime of 2.5 hours, while in other studies they lasted over 6 hours (Young et al. 1995). Entrained air from above the boundary layer into the wake of the downdraft resulted in recovery of the cold pools in the Tompkins study. Timing of the recovery, after the cessation of precipitation and after moisture bottoms out, is roughly the same in both the Tompkins and Young et al. studies.

A four-stage convective life cycle for MCSs was developed from Oklahoma Mesonet cases resulting in cold pools: 1) first storms, 2) MCS initiation, 3) mature MCS, and 4) MCS dissipation (Engerer et al. 2008). A mean potential temperature decrease of 9.5 K and a mean pressure increase of 4.5 mb was found for the first storms life cycle stage with the change in magnitudes dropping slightly throughout the rest of the life cycle.

Oklahoma Mesonet data have also been used to find dozens of bow echo cases (Adams-Selin and Johnson 2010). A conceptual model for bow echoes was produced, showing a similar pressure rise and temperature drop pattern associated with cold pools as was the case for MCSs.

In this study, the pressure and temperature changes at surface Oklahoma Mesonet stations are analyzed for the 1997-2011 period to generate a dataset for a longer climatology. Time series at stations are used due to the 5-minute temporal resolution being preferred over the roughly 40-km spatial resolution of the Oklahoma

Mesonet grid as a means of detecting fronts and cold pools.

Surface divergence is another common feature associated with active cold pools. In this study, cold pool area is defined to include regions of strong surface divergence following a frontal passage, temperature decreases and pressure increases. This definition is more restrictive than that used in other studies of cold pools which include all areas with precipitation or wait until temperature has recovered so cold pools detected with this method would generally be smaller and shorter. The cold pools defined here can be considered to represent regions of active mesoscale cold air mass production due to precipitation. Other parts of a system not defined as a cold pool in this study but likely to be marked as a cold pool in other studies may be considered to be in a residual cold pool.

Section 2 describes the Oklahoma Mesonet dataset in further detail as it relates to this study. Section 3 covers the methodology behind the frontal passage and cold pool analysis. Section 4 details the results from the 15-year climatology of frontal passages and cold pools. The climatology include the changes in temperature and pressure, the convergence/divergence associated with frontal passages, and the seasonal, diurnal, and geographic distribution of frontal passages and cold pools. Section 5 discusses the results while section 6 summarizes the conclusions.

2. Oklahoma Mesonet Dataset

The Oklahoma Mesonet dataset is used in this analysis (Brock et al. 1995; McPherson et al. 2007). The University of Oklahoma and Oklahoma State University are sponsors of the Oklahoma Mesonet. Mesonet observations have been collected since 1994 at 5-minute frequency. Each county of Oklahoma is represented by at least one station, for a total of over 100 stations. These stations are spaced roughly 40 km apart.

Over the years stations have been added but for the purposes of this analysis, only the 113 stations present at the beginning of 1997 are considered. Of these, six were excluded due to residing in the Oklahoma panhandle. Of the remaining stations, each station was used for the years in which observation data for 1.5-m air temperature, 10-m vector average wind magnitude, 10-m vector average wind direction, and station pressure exists for at least 90% of the year. Between 99 and 104 of the 108 non-panhandle stations met the observation threshold each year.

The station resolution of the Oklahoma Mesonet is suitable to resolve large MCS events and their associated cold pools. Smaller systems, such as a cold pool from an individual cumulonimbus cloud, might be missed in the Mesonet data.

3. Methodology

a. Mesonet Grid

Mesonet stations that met the observation threshold for a year were gridded using the Delaunay triangulation procedure (Figure 1). Resulting grids for each year contain some extremely narrow triangles along the border which were removed. Two stations very close to each other located at approximately 35N 98W resulted in two small, narrow triangles that were also removed. Longitude, latitude, and altitude change in the case of a few stations which moved over the 15-year period (1997-2011). These stations were excluded from the grid during the year they moved. Due to the varying number of stations that met the observation threshold each year, and stations that changed location during a year, the grid is adjusted slightly from year to year.

It was also determined that triangles with too long a side length were not representative when it comes to the temporal scales used in the analysis of this study so all triangles with a maximum side length of 80+ km were excluded. This resulted in the removal of 10-13 triangles each year that were primarily along the borders.

b. Divergence

Having identified the grid for the Mesonet domain to be used for each year, near-surface average wind magnitude and direction values are used to determine the divergence in each Mesonet triangle. This calculation is done through the use of equations for the horizontal divergence of triangles on irregular grids (Davies-Jones 1993; Dubois and Spencer 2005). These divergence calculations have been performed for the Oklahoma Mesonet specifically before for divergence analysis (Sun and Krueger 2012).

c. Front Analysis

This study looks at frontal passages as potential indicators for cold pool existence. Previous studies have shown that temperature falls and pressure rises are associated with gust fronts and cold pools (Engerer et al. 2008; Adams-Selin and Johnson 2010). These temperature falls and pressure rises are used to mark the frontal passage. In addition to fronts associated with convective and mesoscale systems, some synoptic fronts can also be detected in the front analysis.

Temperatures at each station were adjusted to remove the diurnal cycle. The diurnal cycle for a station was calculated based on the average temperature for each observation time. An example of an observation time is 10 June 1200 UTC. The average temperature is determined by using all valid temperature measurements at a station during the 15-year period for the observation time as well as all of the observations 24 and 48 hours before and after the observation time at the station (Eq. 1).

$$T_{\mathrm{diur.}} = [\sum_{1997}^{2011} \sum_{\mathrm{day}-2}^{\mathrm{day}+2} T_t]/n \tag{1}$$

In this equation, n is the total number of valid observations and t is the observation time. Without the removal of the diurnal cycle many spurious frontal passages are generated in the analysis in the late afternoon hours as the sun is setting. Similarly, the diurnal cycle was also calculated for the pressure observations (Eq. 2).

$$P_{\text{diur.}} = [\sum_{1997}^{2011} \sum_{\text{day}-2}^{\text{day}+2} P_t]/n \tag{2}$$

Temperature and pressure values were also adjusted to account for elevation with each station adjusted to the Mesonet-averaged elevation, between 365 and 370 m depending on the year since only stations that met the observation threshold for the particular year were included in the average altitude for that year. The temperature values were adjusted by changing the station values dry adiabatically while the pressure values were adjusted using the hypsometric equation. The elevation adjustments had little impact since the differences in adjustment from one observation to the next were very small.

With temperature falls and pressure rises comprising core aspects of gust fronts and cold pools, combining these two variables would provide a useful metric for front strength. The front score (FS) is a unitless variable used in this study to represent the strength of a frontal passage. The FS uses the diurnal- and elevation-adjusted temperature falls and pressure rises over 30-minute intervals, calculated every 5 minutes. For example, the FS at 1230 UTC uses the changes in adjusted temperature and pressure between 1200 UTC and 1230 UTC. A 1 mb pressure increase is treated the same as a 1 K temperature fall. Later, observations will show that temperature falls tend to be larger than pressure rises; however, temperature is often used in other studies as a cold pool initiation or ending signal so it is given a higher relative weight here. Adding these changes yields the FS (Eq. 3). An example of FSs at a station over a season is shown for JJA 1997 at the Blackwell Mesonet station (Figure 2).

$$FS_{\text{final}} = 1\,\text{mb}^{-1}\Delta P_{\text{diur.,elev.}} - 1\,\text{K}^{-1}\Delta T_{\text{diur.,elev.}} \tag{3}$$

FSs are used to identify whether a frontal passage occurs at a Mesonet station or triangle. A front is considered to have reached a Mesonet station when the FS at the station exceeds a threshold. Also, the FS at the station must be the highest it reaches within 3 hours in either direction in order to identify the primary front associated with a system. FSs of 3 and 5 are used as thresholds for fronts and strong fronts, respectively. The 30-minute period generating the highest FS value for a front is, in the vast majority of cases, also the first 30-minute period in which a FS exceeded the threshold value.

A frontal passage at a Mesonet triangle is determined to have occurred if all three stations that comprise the triangle corners experience a frontal passage within a 2-hour span. The 2-hour limit is the reason for limiting maximum triangle side length to 80 km since slower fronts would be less likely to be detected in larger triangles leading to an underestimate in frontal passage frequency. However, extending the 2-hour limit would have captured more spurious fronts. The duration of a frontal passage at a triangle is the time elapsed from when the first corner is reached until the time when the last corner is reached. The fronts can be tracked across the Mesonet as they progress through Oklahoma.

d. Cold Pool Analysis

The front analysis is necessary for determining the location of potential cold pools since a gust front marks the leading edge of a cold pool (Wakimoto 1982). Cold pools are primarily identified by temperature falls and pressure rises, as was the case for the frontal passages in the previous section. Additionally, active cold pools are regions of surface divergence, which is an identifier used in this study to isolate fronts associated with active cold pools from other frontal passages. As a result, *cold pool boundaries are defined in this study by Mesonet triangles with surface divergence following a frontal passage*. This definition is more limiting than those that are generally used for which continuing precipitation and/or a lack of surface temperature recovery indicates a sustained cold pool. The cold pools in this Oklahoma Mesonet study are representative of regions in which a cold air mass is expanding or building via precipitation processes such as evaporative cooling whereas other studies use areas of cold air persistence due to a lack of surface heating. Precipitation is necessary for evaporative cooling, though the precipitation does not have to reach the ground for evaporative cooling to occur. Dry frontal passages generally did not result in cold pools in our cold pool analysis due to insufficiently large divergence values.

A cold pool occurs at a Mesonet triangle if the triangle experiences a frontal passage and if the 15-minute averaged strong divergence threshold ($D_i > 10^{-4}\mathrm{s}^{-1}$) is met within half an hour before or an hour after the frontal passage propagates halfway through the triangle. The longer time duration after the frontal passage recognizes that cold pools follow gust fronts. It is possible, given the resolution of the Mesonet grid, that a cold pool could seemingly be slightly ahead of a front which would indicate a strong cold pool covering less than half the triangle area. When a cold pool is determined to have occurred, the duration of the cold pool at the triangle is calculated. This is done by finding the divergence maximum and the timesteps before and after when the divergence falls below half the maximum divergence value for the triangle. Fronts and cold pools can be tracked across the Mesonet giving a detailed view of the analysis for case studies and cold pool areas, noted in detail in Part II.

4. 15-year Climatology of Fronts and Cold Pools

The 1997-2011 period of Oklahoma Mesonet data was analyzed for frontal passages and cold pools and statistics were gathered. Frontal passage and cold pool statistics are now presented for: (1) Temperature and pressure changes, (2) Convergence/divergence, (3) Seasonal distribution, (4) Diurnal distribution, and (5) Geographic distribution.

a. Temperature and Pressure Changes

For each frontal passage at a Mesonet triangle, all three corner stations of the triangle were included in the statistics of changes in temperature and pressure. The changes in these variables during all frontal passages (FS3+), strong frontal passages (FS5+), all frontal passages which resulted in cold pools, and strong frontal passages which resulted in cold pools are shown (Table 1).

The temperature difference is calculated by subtracting the lowest temperature within 2 hours after the frontal passage at a station from the highest temperature within 30 minutes before a frontal passage. Pressure differences are calculated by subtracting the lowest pressure within 30 minutes before the frontal passage at a station from the highest pressure within 2 hours after a frontal passage.

Generally, results for all frontal passages were similar to those for fronts that led to cold pools. The magnitude of both variable changes are slightly higher on average for fronts with cold pools compared to all fronts (FS3+). For strong fronts the converse is the case with strong fronts yielding slightly higher average variable changes than strong fronts resulting in cold pools.

Average temperature falls are lower in magnitude in spring and higher in magnitude in winter. Average pressure rises have a distinct minimum in magnitude in summer while the winter pressure changes are largest on average.

For individual stations, ΔT and ΔP show low correlation, -0.28, with fronts primarily taking the form of 3-7 K temperature drops and 0-4 mb pressure rises (Figure 3). Correlations were calculated for all fronts and for fronts with cold pools for each season (Table 2). The correlations did not change significantly when fronts without cold pools were left out. Likewise, using only strong fronts made little change in the correlations. Summer correlations were near 0 while winter and spring had the highest correlations. The reason for the extremely low correlations in the summer, particularly for strong fronts, is likely a result of the differing types of precipitating systems the region receives each season. Isolated convective thunderstorms are more common in the summer than the spring where synoptic events are more likely. Stratiform precipitation events are more likely to occur in non-summer months and are more uniform in structure than their convective counterparts.

b. Convergence/Divergence

It is expected for convergence to occur ahead of a frontal passage and divergence behind a frontal passage. Cold pools are marked by the presence of significant divergence associated with a frontal passage, generally shortly after a frontal passage occurs. The divergence values were averaged over 15 minutes to smooth out timing discrepancies that may occur in a study like ours with large station spacing.

The divergence values were calculated at the beginning, middle, and end of each triangle's frontal passages. The beginning of the frontal passage is defined as the timestep when the first corner of a Mesonet triangle experiences a local maximum FS. The end of the frontal passage is defined as the timestep when the third corner of a Mesonet triangle experiences a local maximum FS. The middle is the timestep halfway between the beginning and end or, if there is an even number of timesteps in between, the average of the two middle divergence values.

The average divergence values for all frontal passages are listed in (Table 3). On average, as a front reaches a Mesonet triangle, the triangle had strong convergence ($D_i < -10^{-4}$ s^{-1}). The magnitude of convergence varied slightly from season to season with convergence for all fronts being slightly weaker in winter and convergence for strong fronts slightly stronger in spring and fall. For fronts at the middle of a triangle, there was a large seasonal difference. Summer frontal passages had divergence on average while the other three seasons maintained convergence as a front reached the middle of a triangle. At the end of a frontal passage, summer had the strongest divergence on average, a factor of 2 larger than spring and fall, and a factor of 5 larger than winter. This is largely attributable to the much stronger convective downdrafts that occur far more frequently in the summer than in the winter when stratiform precipitation is dominant. End-of-front divergence in summer was roughly the same magnitude as beginning-of-front convergence. For the other three seasons the magnitude of convergence at the beginning of a frontal passage was much larger than the magnitude of divergence at the end of a frontal passage.

Divergence values for frontal passages which yielded cold pools are shown in (Table 4). Because cold pools require the divergence threshold to be exceeded, the end divergence and middle divergence values are much larger than for all frontal passages. However, the seasonal pattern remains the same with summer having the highest divergence values for the middle and end of frontal passages and winter having the lowest convergence at the beginning of frontal passages and lowest divergence at the end of frontal passages. It is notable that the beginning divergence values are roughly the same for cold pools as for all frontal passages. This suggests that divergence behind a front is not significantly related to the strength of convergence ahead of a front.

c. *Seasonal Distribution*

The seasonal distribution of frontal passages and cold pools was also determined. For this calculation, instead of the station data of each triangle that experienced a front or cold pool being used, it is the data from triangles that experienced a front or cold pool (Table 5). There were more cold pools during the summer than the other seasons while frontal passages were similar for spring and summer. Winter had the fewest number of front and cold pools. The dominance of spring and summer matches up well with increased convective activity in the region, an example of which is the heightened frequency of tornadoes during that period. Frontal passages during the summer also had the highest percentage of fronts leading to cold pools. Stronger fronts resulted in higher odds of cold pool formation, as expected.

A factor that influences the seasonal differences is the dependence of precipitation evaporation on temperature. An increase in temperature leads to an increase in precipitation evaporation. As a result, summer months are more highly influenced by precipitation evaporation which explains a portion of the seasonal difference, particularly for cold pools. Additionally, seasonal variation between convective and stratiform precipitation is likely an influence in this result. During the summer heavier precipitation events in convective storms are much more frequently occurring than during the winter. Stronger updrafts and downdrafts are associated with these events which in turn result in stronger gust fronts and higher divergence in the cold pool region.

d. Diurnal Distribution

The diurnal distributions of frontal passages and cold pools were calculated by summing the number of fronts at all triangles over hourly periods (0000-0055 UTC, 0100-0155 UTC,..., 2300-2355 UTC). Seasons were defined as: MAM for spring, JJA for summer, SON for fall, and DJF for winter.

There is a significant seasonal variation in the diurnal distribution of frontal passages (Figure 4). In the summer (Figure 4b) there is a large peak in frontal passage frequency in the afternoon, from 20-01 UTC (14-19 LST), with frontal passage frequencies twice as high as the rest of the day. The other three seasons have much smaller variation in the diurnal cycle.

The standard deviations are quite large, and due to the non-Gaussian nature of the distribution, reach below zero in some instances. This comes from the tendency for frontal passages to largely occur at the same time of day for a given system moving through Oklahoma because a single synoptic front can sweep through many of the triangles within a few hours. Despite it being impossible for there to be more strong frontal passages than total fronts in a given year, the standard deviations overlap which means it can be expected that some years have more strong fronts in a given hour of the day than other years have total fronts in that hour.

The diurnal distribution of cold pool frequency (not shown) is very similar to that for frontal passages. For frontal passages and cold pools the differences between the highest and lowest average frequencies for spring, summer, and fall, are around 50% while for summer the difference is over 200%.

The percentage of frontal passages with cold pools was also calculated for the diurnal cycle (Figure 5). For most hours of the day in each of the four seasons, the percentage of strong fronts with cold pools was higher than the percentage of all fronts with cold pools. Consistently throughout the year, the evening hours, 00-06 UTC (18-00 LST), had the largest spread between all and strong frontal passages leading to cold pools.

In spring (Figure 5a) roughly 60% of fronts resulted in cold pools throughout most of the day. The morning hours were the exception with the percentage dropping below 50% for several hours (15-19 UTC). In summer (Figure 5b) had the highest rate of frontal passages yielding cold pools, exceeding 90% in the evening hours for strong frontal passages. No individual hour during summer falls below 70% of total fronts yielding cold pools. There is a slighter drop in the percentage of frontal passages with cold pools in the morning hours for summer than for spring, and this drop did not occur for strong frontal passages. In the fall evening hours (Figure 5c) 60% of frontal passages and 75% of strong frontal passages resulted in cold pools. During the day these percentages fell to between 40 and 55% until the mid-afternoon. In the winter (Figure 5d) the rate of frontal passages resulting in cold pools is uniform throughout the day between 30 and 40%, a rate less than half as high as it is for summer.

e. Geographic Distribution

Finally, the geographic distributions of frontal passages and cold pools across the Mesonet were computed. Linear regressions were performed using a least-squares fit to determine the dependence of triangle frequencies on triangle area and maximum side length. The frequencies regressions were calculated for include all fronts, strong fronts, cold pools, and cold pools following strong fronts (Table 6).

Triangles with larger areas and larger maximum side lengths had lower frequencies of frontal passages and cold pool occurrence on average. This was expected since all three triangle corners have to be crossed to trigger a frontal passage for the triangle. With small, isolated thunderstorm events this is less likely to be captured on portions of the grid with lower resolution, as well as very slow moving storms that fail to reach all three corners within 2 hours.

Each triangles' frontal passage and cold pool frequency was adjusted using these regression lines by first calculating the y-intercept using: 1) the same slope as the Mesonet regression line, 2) the triangle area or maximum side length, and 3) the number of frontal passages/cold pools for a given triangle. Then the adjusted number of frontal passages/cold pools are calculated using: 1) the same slope as the Mesonet regression line, 2) the calculated y-intercept, and 3) the average area/average maximum side length for the Mesonet. The frontal passage/cold pool frequency adjusted by area and the frontal passage /cold pool frequency adjusted by maximum side length were averaged together to incorporate both effects and finally smoothed using a Barnes analysis with a half degree smoothing length scale. The end result of these adjustment is the geographic distribution of front frequencies (Figure 6) and cold pool frequencies (Figure 7) displayed.

For the frontal passage frequencies a west to east gradient is apparent with western regions of Oklahoma observe larger frequencies of frontal passages than eastern regions of Oklahoma (Figure 6a). Strong fronts adjusted by area (Figure 6b) show a similar distribution. In both cases the highest frequencies are in the northwest and the lowest frequencies in the southeast.

For the cold pool frequencies the west to east gradient is similar but weaker than it is for frontal passages (Figure 7a). Western areas have the highest cold pool frequencies while the northeast and southeast have the lowest average frequencies of cold pools. There is less uniformity to the pattern for cold pools with more isolated areas of higher or lower frequencies. Cold pools resulting from strong fronts (Figure 7b) show roughly the same geographic frequency pattern as all cold pools.

5. Discussion

The results detailed in the preceding chapter extend analysis of Oklahoma Mesonet data to a 15-year dataset, providing a much larger sample size for seasonal analyses of frontal passages and convective cold pools. This allows for clearer signals to appear in the data with increased certainty that the results obtained therein are representative.

The correlation of ΔT with ΔP was near 0 during the summer with -0.04 for strong summer fronts that led to cold pools. This suggests that the vertical structure of the temperature perturbation in the cold pools varies significantly from case to case. The variations in structure are expected to be larger in convective systems rather than in stratiform precipitation systems due to deeper and more varied updraft, boundary layer, and cold pool heights. Three-dimensional data would aid in resolving the vertical features in the Mesonet. For this reason, case studies involving intense observations periods (IOPs) are the most productive to pursue in future research. The MC3E period is one such IOP that would have an enhanced capacity to resolve 3D structure for cases.

Studies have observed pressure and temperature changes in cold pool cases. In one such study (Engerer et al. 2008) the average pressure rise in cold pools from 39 MCS events between April and August was 4.5

mb while the average temperature fall was 9.5 K. It is safe to assume that these MCS events were chosen because they were particular strong so the comparison for the 15-year dataset would be strong fronts which averaged a 3.6-mb pressure rises in spring, a 2.5-mb pressure rises in summer, and a 7.7-K temperature drops in both spring and summer. Though the Engerer et al. study found larger pressure and temperature changes on average, considering the that 15-year dataset was diurnally adjusted, and the much larger sample size for 15-year dataset of strong fronts that may be weighted down with weaker, albeit still strong, fronts, the results are in reasonable agreement.

The geographical distribution of frontal passages suggests a west to east gradient with a higher frequency of frontal passages on the westward side of Oklahoma. One possible influence is the dryline which frequently develops in the lee of the Rocky Mountains and advances into Oklahoma where numerous case studies have been made over the years (McCarthy and Koch 1982; Ziegler and Hane 1993; Buban et al. 2007). A climatology of springtime dryline position matches well with the frontal passage geographic distribution anomaly pattern (Hoch and Markowski 2005). Their Figure 2 showed that the dryline most frequently was located around 101W longitude and the dryline location range is generally from 103W to 97W with rare occurrences farther eastward. The west to east pattern is weaker when it comes to cold pools, possibly suggesting that western stations have a higher rate of frontal passages not resulting in cold pools.

6. Conclusions

A 15-year climatology of Oklahoma Mesonet frontal passages and convective cold pools was created and analyzed. This is the first long-term climatology of convective cold pools. Previous studies involving cold pools in the Oklahoma Mesonet have looked at shorter time periods with a focus on other features such as mesoscale convective complexes (MCSs) (Engerer2008) and squall lines (AdamsSelin2010).

Frontal passages were identified by determining when Mesonet stations experienced a front. A non-dimensional variable, the front score (FS), was derived using 30-minute temperature falls and pressure rises. When all three stations in a Mesonet triangle experience a frontal passage within 2 hours a front occurs at the Mesonet station and can be tracked. A cold pool event required a frontal passage to occur at a Mesonet triangle and for the divergence of the triangle to exceed the threshold value of $> 10^{-4}\mathrm{s}^{-1}$ within half an hour before or an hour after the frontal passage is halfway through the triangle.

Convective cold pools feature a temperature fall, a pressure rise, and surface divergence as a result of evaporative precipitation processes. The associated gust front features convergence ahead of the front and divergence behind the front. The frontal passage and cold pool results suggested a tendency for synoptic scale fronts without surface precipitation to not be associated with areas of strong divergence. Alternatively, fronts associated with MCSs resulted in precipitation and a mesoscale divergence region at the surface. However, there are exceptions to both types in the analysis.

Changes in temperature and pressure during frontal passages were determined. Spring had the smallest average magnitude of ΔT while summer had the smallest average magnitude of ΔP. Both variables had their largest average magnitude changes in the winter. Correlations between ΔT and ΔP were low, -0.28, with near 0 correlation in summer and highest in winter and spring ($\sim$0.4). This result indicates a large variety in vertical structure of the temperature perturbations accompanying cold pools. The average change and their correlation was generally similar for fronts with cold pools and for all fronts.

Convergence values ahead of frontal passages were mostly similar for all seasons. However, summer frontal passages transitioned to divergence quicker, and had much larger divergence values as a front finished crossing a Mesonet triangle than was the case for the other seasons, especially winter.

Seasonally, spring and summer had the highest frequency of frontal passages (over 22,000 fronts and 8,000 strong fronts), while summer had the highest frequency of cold pools and the percentage of frontal passages which resulted in cold pools (79% of fronts and 87% of strong fronts). Winter was lowest in all three categories with roughly half as many fronts, a quarter as many cold pools and only 35% of fronts and 40% of strong fronts resulting in cold pools.

The diurnal cycle of fronts and cold pools has a strong seasonal variation. During the summer, frontal passages and cold pools are most frequent in the late afternoon to evening hours, coinciding with daytime-heating-induced convection, over twice as often as the other hours ($\sim$130 vs $\sim$50 per year). The other seasons have much smaller diurnal variation in frontal passage and cold pool frequency. The summer pattern is the dominant influence on the annual pattern for the diurnal cycle.

Geographically, the size of Mesonet triangles, in terms of area and maximum side length, has a significant influence on the analyzed frequency of frontal passages and cold pools. After this analysis artifact is accounted for, it is evident that western regions of Oklahoma experienced higher frequencies of frontal passages in particular, and cold pools to a lesser degree, than eastern regions.

The methods used in this analysis can be applied to simulations using models such as the Weather Research and Forecasting (WRF) model and the System for Atmospheric Modeling (SAM). Particularly useful would be the increased resolution in a model relative to the Oklahoma Mesonet. A higher resolution would improve representations, especially for cases of smaller scale features and isolated convection that can be missed on grids with 40-km spacing.

The Mesonet observations resided in only two spatial dimensions. Obtaining three-dimensional data, whether observationally or with model output, would improve understanding of the reasons behind the low correlations between changes in pressure and temperature during frontal passages, particularly in the summer. The MC3E field campaign produced an extensive set of data from which case studies can be analyzed in three dimensions.

Estimating rain evaporation from surface pressure anomalies in cloud-resolving model simulations could be used to develop a method to implement in cold pool analysis. Fujita had developed methods to calculate rain evaporation which assumed that the entirety of the pressure rise was a result of evaporated precipitation (Fujita 1959). Comparing rain evaporation estimates to rain evaporation derived from cloud-resolving model (CRM) simulations can better identify the method best suited for developing rain evaporation estimates using only surface observations.

Additionally, these results could be used to evaluate cold pool parameterizations in global climate models (GCMs). Identifying regions of cold air production at the surface due to precipitation evaporation and surface outflow boundaries could lead to an improved predictability in new cell formation, cold pool longevity, and outflow structures.

Furthering the understanding of cold pools can lead to better representation in numerical weather prediction models, as well as improved analysis of gust fronts, squall lines, MCSs and other features associated with convection. Improved tracking of mesoscale and synoptic conditions, in turn, would lead to increased preparedness when it comes to severe weather events.

Acknowledgments.

This research was supported by the Office of Science (BER), U.S. Department of Energy, Grant No. DE-FG02-08ER64553. Data were obtained from the Atmospheric Radiation Measurement (ARM) Program sponsored by the U.S. Department of Energy, Office of Science, Office of Biological and Environmental Research, Climate and Environmental Sciences Division. Oklahoma Mesonet data are from a cooperative venture between Oklahoma State University and The University of Oklahoma, supported by the taxpayers of Oklahoma.

REFERENCES

Adams-Selin, R. D. and R. H. Johnson, 2010: Mesoscale surface pressure and temperature features associated with bow echoes. *Mon. Wea. Rev.*, **138**, 212–227.

Brock, F. V., K. C. Crawford, R. L. Elliott, G. W. Cuperus, S. J. Stadler, H. L. Johnson, and M. D. Eilts, 1995: The Oklahoma Mesonet: A technical overview. *J. Atmos. Oceanic. Technol.*, **12**, 5–19.

Buban, M. S., C. L. Ziegler, E. N. Rasmussen, and Y. P. Richardson, 2007: The dryline on 22 May 2002 during IHOP: Ground-radar and in situ data analyses of the dryline and boundary layer evolution. *Mon. Wea. Rev.*, **135**, 2473–2505.

Davies-Jones, R., 1993: Useful formulas for computing divergence, vorticity, and their errors from three or more stations. *Mon. Wea. Rev.*, **121**, 1449–1458.

Dubois, J. A. and P. L. Spencer, 2005: Computing divergence from a surface network: Comparison of the triangle and pentagon methods. *Wea. Forecasting*, **20**, 596–608.

Engerer, N. A., D. J. Stensrud, and M. C. Coniglio, 2008: Surface characteristics of cold pools. *Mon. Wea. Rev.*, **136**, 4839–4849.

Fujita, T., 1955: Results of detailed synoptic studies of squall lines. *Tellus*, **7**, 405–436.

Fujita, T., 1959: Precipitation and cold air production in mesoscale thunderstorm systems. *J. Meteor.*, **16**, 454–466.

Hoch, J. and P. M. Markowski, 2005: A climatology of springtime dryline position in the U.S. Great Plains region. *J. Climate*, **18**, 2132–2137.

Markowski, P. M. and Y. P. Richardson, 2012: *Mesoscale Meteorology in Midlatitudes.* Wiley-Blackwell, 407 pp.

McCarthy, J. and S. E. Koch, 1982: The evolution of an Oklahoma dryline. Part I: A meso- and subsynoptic-scale analysis. *J. Atmos. Sci.*, **39**, 225–236.

McPherson, R. A., et al., 2007: Statewide monitoring of the mesoscale environment: A technical update on the Oklahoma Mesonet. *J. Atmos. Oceanic Technol.*, **24**, 301–321.

Newton, C. W., 1950: Structure and mechanism of the prefrontal squall line. *J. Meteor.*, **7**, 210–222.

Roux, F., 1988: The West African squall line observed on 23 June 1981 during COPT81: Kinematics and thermodynamics of the convective region. *J. Atmos. Sci.*, **45**, 406–426.

Seigel, R. B. and S. C. van den Heever, 2012: Simulated density currents beneath embedded stratified layers. *J. Atmos. Sci.*, **69**, 2192–2200.

Stensrud, D. J. and J. M. Fritsch, 1994: Mesoscale convective systems in weakly forced large-scale environments. Part II: Generation of a mesoscale initial condition. *Mon. Wea. Rev.*, **122**, 2068–2083.

Stensrud, D. J., G. S. Manikin, E. Rogers, and K. E. Mitchell, 1999: Importance of cold pools to NCEP mesoscale Eta model forecasts. *Wea. Forecasting*, **14**, 650–670.

Sun, R. and S. K. Krueger, 2012: Mesoanalysis of the interactions of precipitating convection and the boundary layer. *J. Adv. Model. Earth Syst.*, **4**, DOI: 10.1029/2011MS000 096.

Tepper, M., 1950: A proposed mechanism of squall lines: The pressure jump line. *J. Meteor.*, **7**, 21–29.

Tompkins, A. M., 2001: Organization of tropical convection in low vertical wind shears: The role of cold pools. *J. Atmos. Sci.*, **58**, 1650–1672.

Wakimoto, R. M., 1982: The life cycle of thunderstorm gust fronts as viewed with Doppler radar and rawinsonde data. *Mon. Wea. Rev.*, **110**, 1060–1082.

Weisman, M. L. and R. Rotunno, 2005: Reply. *J. Atmos. Sci.*, **62**, 2997–3002.

Young, G. S., S. M. Perugini, and C. W. Fairall, 1995: Convective wakes in the equatorial western Pacific during TOGA. *Mon. Wea. Rev.*, **123**, 110–123.

Ziegler, C. L. and C. E. Hane, 1993: An observational study of the dryline. *Mon. Wea. Rev.*, **121**, 1134–1151.

List of Tables

1 Average ΔT and ΔP for all frontal passages (fp, FS3+ / FS5+) and for frontal passages resulting in cold pools (cp, FS3+/FS5+). 25

2 Correlations between ΔT and ΔP for all frontal passages (fp, FS3+ / FS5+) and for frontal passages which yield cold pools (cp, FS3+ / FS5+). 26

3 Divergence values at the beginning, middle, and end of all triangle frontal passages experienced by Mesonet triangles from 1997-2011 by season (FS3+ / FS5+) in s^{-1}. 27

4 Divergence values at the beginning, middle, and end of triangle frontal passages yielding cold pools experienced by Mesonet triangles from 1997-2011 by season (FS3+ / FS5+) in s^{-1}. 28

5 Number of frontal passages and cold pools experienced by Mesonet triangles from 1997-2011 by season (FS3+ / FS5+). 29

6 Linear regression formulas (triangle area in km^2, triangle max side length in km). 30

TABLE 1. Average ΔT and ΔP for all frontal passages (fp, FS3+ / FS5+) and for frontal passages resulting in cold pools (cp, FS3+/FS5+).

Season	**ΔT (K) fp**	**ΔP (mb) fp**	**ΔT (K) cp**	**ΔP (mb) cp**
Spring (MAM)	-5.8/-7.7	2.8/3.6	-5.8/-7.5	2.9/3.5
Summer (JJA)	-6.1/-7.7	2.0/2.5	-6.2/-7.7	2.0/2.5
Fall (SON)	-6.2/-8.4	2.4/3.1	-6.3/-8.3	2.6/3.1
Winter (DJF)	-6.6/-10.2	2.9/4.4	-7.1/-10.3	3.5/4.5
Annual	-6.1/-8.1	2.5/3.2	-6.2/-8.0	2.6/3.1

TABLE 2. Correlations between ΔT and ΔP for all frontal passages (fp, FS3+ / FS5+) and for frontal passages which yield cold pools (cp, FS3+ / FS5+).

Season	**ΔT,ΔP fp**	**ΔT,ΔP cp**
Spring (MAM)	-0.32/-0.44	-0.32/-0.46
Summer (JJA)	-0.15/-0.06	-0.13/-0.04
Fall (SON)	-0.23/-0.17	-0.22/-0.18
Winter (DJF)	-0.41/-0.38	-0.44/-0.43
Annual	-0.28/-0.32	-0.27/-0.32

TABLE 3. Divergence values at the beginning, middle, and end of all triangle frontal passages experienced by Mesonet triangles from 1997-2011 by season (FS3+ / FS5+) in s^{-1}.

Season	Beg. Div.	Mid. Div.	End. Div.
Spring (MAM)	-1.40E^{-4}/-2.00E^{-4}	-1.55E^{-5}/-2.55E^{-5}	6.50E^{-5}/8.08E^{-5}
Summer (JJA)	-1.32E^{-4}/-1.72E^{-4}	1.87E^{-5}/2.47E^{-5}	1.24E^{-4}/1.61E^{-4}
Fall (SON)	-1.37E^{-4}/-2.02E^{-4}	-3.12E^{-5}/-5.30E^{-5}	5.75E^{-5}/8.03E^{-5}
Winter (DJF)	-1.09E^{-4}/-1.75E^{-4}	-3.52E^{-5}/-6.36E^{-5}	2.30E^{-5}/2.94E^{-5}
Annual	-1.32E^{-4}/-1.87E^{-4}	-1.10E^{-5}/-1.83E^{-5}	7.50E^{-5}/1.01E^{-4}

TABLE 4. Divergence values at the beginning, middle, and end of triangle frontal passages yielding cold pools experienced by Mesonet triangles from 1997-2011 by season (FS3+ / FS5+) in s^{-1}.

Season	**Beg. Div.**	**Mid. Div.**	**End. Div.**
Spring (MAM)	$-1.35E^{-4}/-1.86E^{-4}$	$3.47E^{-5}/2.77E^{-5}$	$1.26E^{-4}/1.36E^{-4}$
Summer (JJA)	$-1.29E^{-4}/-1.70E^{-4}$	$4.69E^{-5}/4.63E^{-5}$	$1.62E^{-4}/1.89E^{-4}$
Fall (SON)	$-1.35E^{-4}/-1.98E^{-4}$	$2.11E^{-5}/1.90E^{-6}$	$1.27E^{-4}/1.45E^{-4}$
Winter (DJF)	$-9.82E^{-5}/-1.62E^{-4}$	$2.51E^{-5}/4.22E^{-5}$	$9.58E^{-5}/9.66E^{-5}$
Annual	$-1.29E^{-4}/-1.78E^{-4}$	$3.68E^{-5}/3.02E^{-5}$	$1.38E^{-4}/1.58E^{-4}$

TABLE 5. Number of frontal passages and cold pools experienced by Mesonet triangles from 1997-2011 by season (FS3+ / FS5+).

Season	**# Fronts**	**# Cold Pools**	**% Fronts w/ Cold Pools**
Spring (MAM)	23,811/8,329	13,820/5,397	58%/65%
Summer (JJA)	22,785/9,014	18,083/7,855	79%/87%
Fall (SON)	13,009/4,442	6,645/2,620	51%/59%
Winter (DJF)	12,539/3,843	4,329/1,530	35%/40%
Annual	72,144/25,628	42,877/17,402	59%/68%

TABLE 6. Linear regression formulas (triangle area in km^2, triangle max side length in km).

y	Area Adjustment	Length Adjustment
All Fronts$_{FS3+}$	y = -7.9E$^{-3}\times$ Triangle Area + 34	y = -0.27 $\times$ Triangle Max Side Length + 43
Strong Fronts$_{FS5+}$	y = -3.2E$^{-3}\times$ Triangle Area + 13	y = -0.10 $\times$ Triangle Max Side Length + 16
Cold Pools$_{FS3+}$	y = -1.1E$^{-2}\times$ Triangle Area + 26	y = -0.26 $\times$ Triangle Max Side Length + 31
Cold Pools$_{FS5+}$	y = -4.1E$^{-3}\times$ Triangle Area +10	y = -0.10 $\times$ Triangle Max Side Length +12

List of Figures

1 Map of the Oklahoma Mesonet grid used for 1997. Delaunay triangulation was used to interpolate the points onto the grid and particularly long and skinny triangles were removed. Removed triangles were primarily on the outer border with the exception of two near 98W and 35N. 32

2 Front scores for the JJA 1997 period at the Blackwell Mesonet station (36.75N, 97.25W). High, positive front scores indicate frontal passages. 33

3 ΔP vs ΔT for all frontal passages at triangles in the Oklahoma Mesonet from the 1997-2011 period. The colorbar represents the frequency of occurrence. The correlation is -0.28. 34

4 Seasonally averaged diurnal cycle (in UTC time) of all frontal passages at triangles in the Oklahoma Mesonet from the 1997-2011 period along with standard deviations. Results are shown for (a) spring, (b) summer, (c), fall, and (d) winter for all frontal passages (red) and strong frontal passages (blue). 35

5 Seasonally averaged diurnal cycle (in UTC time) of the percentage of all (red) and strong (blue) fronts that yield cold pools. Results are shown for (a) spring, (b) summer, (c), fall, and (d) winter for all frontal passages (red) and strong frontal passages (blue). 36

6 Geographic distribution of (a) all frontal passages and (b) strong frontal passages. Frontal passage frequencies were adjusted using Mesonet triangle areas and maximum side lengths, then smoothed using a Barnes analysis. 37

7 Geographic distribution of (a) all cold pools and (b) cold pools following strong frontal passages. Cold pool frequencies were adjusted using Mesonet triangle areas and maximum side lengths, then smoothed using a Barnes analysis. 38

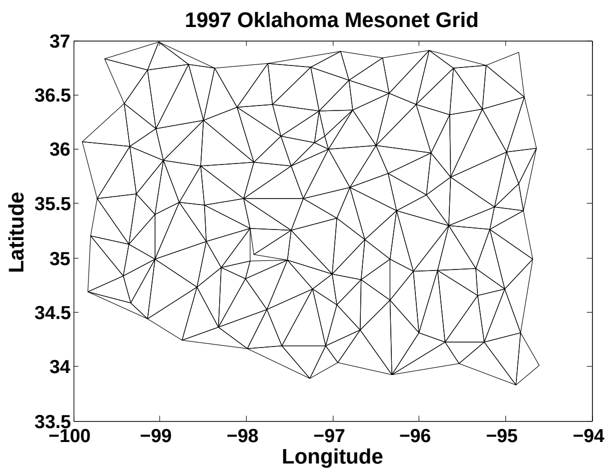

FIG. 1. Map of the Oklahoma Mesonet grid used for 1997. Delaunay triangulation was used to interpolate the points onto the grid and particularly long and skinny triangles were removed. Removed triangles were primarily on the outer border with the exception of two near 98W and 35N.

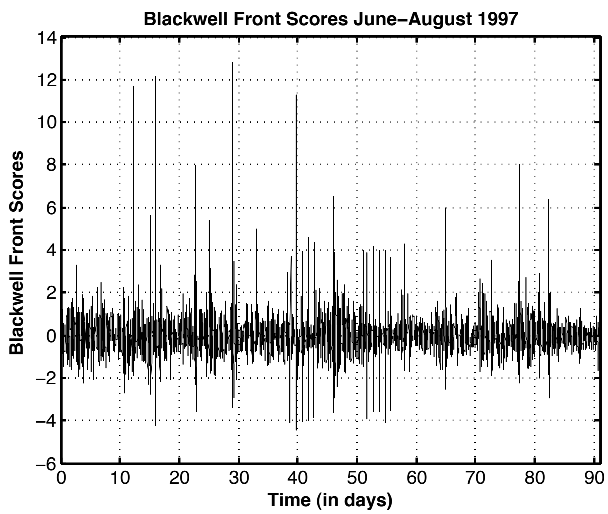

FIG. 2. Front scores for the JJA 1997 period at the Blackwell Mesonet station (36.75N, 97.25W). High, positive front scores indicate frontal passages.

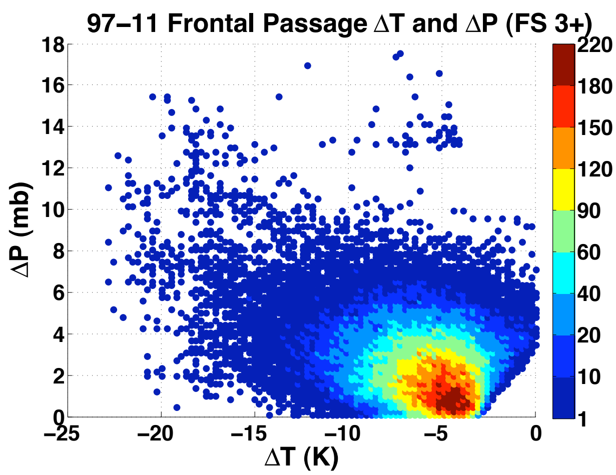

FIG. 3. ΔP vs ΔT for all frontal passages at triangles in the Oklahoma Mesonet from the 1997-2011 period. The colorbar represents the frequency of occurrence. The correlation is -0.28.

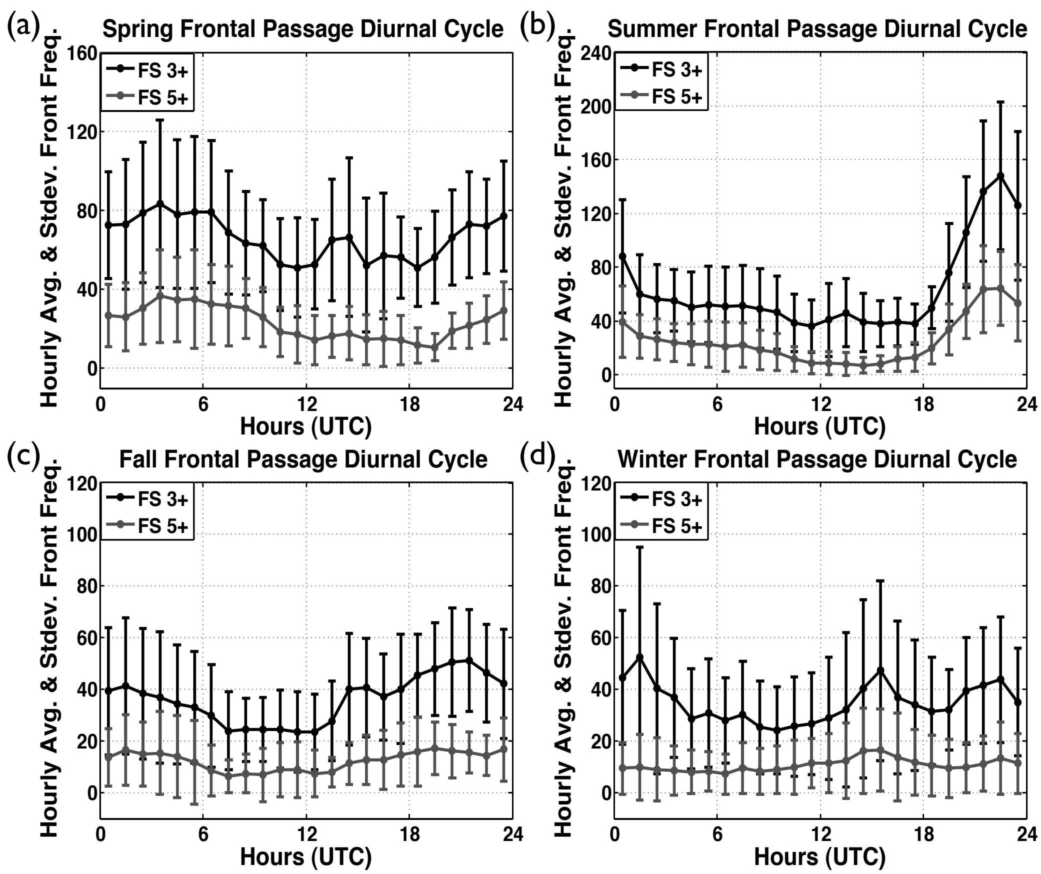

FIG. 4. Seasonally averaged diurnal cycle (in UTC time) of all frontal passages at triangles in the Oklahoma Mesonet from the 1997-2011 period along with standard deviations. Results are shown for (a) spring, (b) summer, (c), fall, and (d) winter for all frontal passages (red) and strong frontal passages (blue).

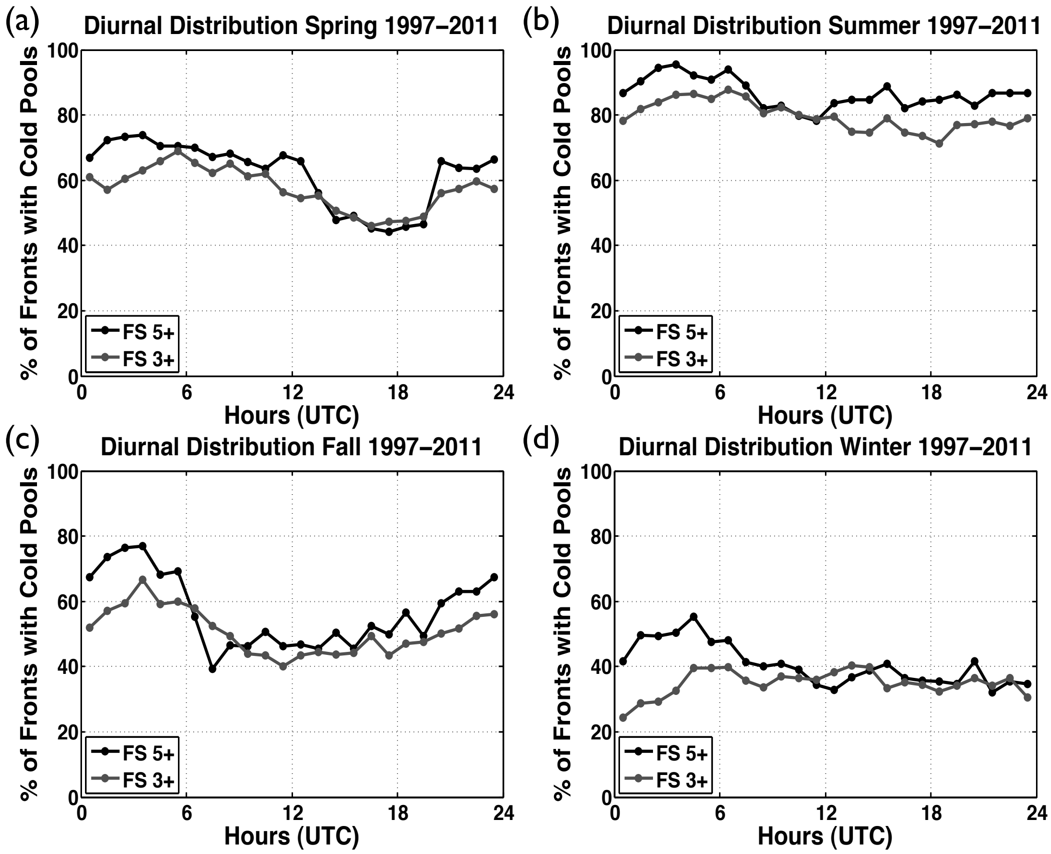

FIG. 5. Seasonally averaged diurnal cycle (in UTC time) of the percentage of all (red) and strong (blue) fronts that yield cold pools. Results are shown for (a) spring, (b) summer, (c), fall, and (d) winter for all frontal passages (red) and strong frontal passages (blue).

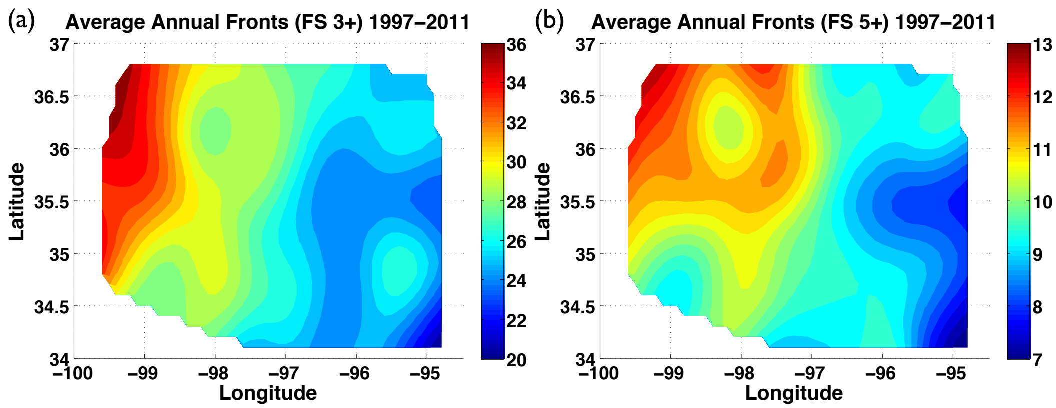

FIG. 6. Geographic distribution of (a) all frontal passages and (b) strong frontal passages. Frontal passage frequencies were adjusted using Mesonet triangle areas and maximum side lengths, then smoothed using a Barnes analysis.

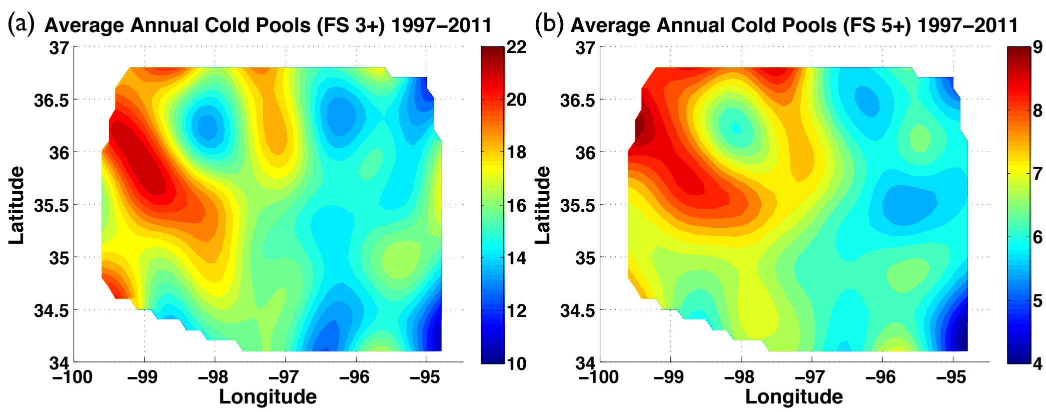

FIG. 7. Geographic distribution of (a) all cold pools and (b) cold pools following strong frontal passages. Cold pool frequencies were adjusted using Mesonet triangle areas and maximum side lengths, then smoothed using a Barnes analysis.